Stenoparib, an Inhibitor of Cellular Poly(ADP-Ribose) Polymerase, Blocks Replication of the SARS-CoV-2 and HCoV-NL63 Human Coronaviruses *In Vitro*

Nathan E. Stone,[a] Sierra A. Jaramillo,[a] Ashley N. Jones,[a] Adam J. Vazquez,[a] Madison Martz,[a] Lora M. Versluis,[a,b]
Marlee O. Raniere,[a,b] Haley E. Nunnally,[a] Katherine E. Zarn,[a] Roxanne Nottingham,[a] Ken R. Ng,[a] Jason W. Sahl,[a,b]
⏺ David M. Wagner,[a,b] Steen Knudsen,[c] Erik W. Settles,[a,b] ⏺ Paul Keim,[a,b] Christopher T. French[a,b]

[a]Pathogen and Microbiome Institute, Northern Arizona University, Flagstaff, Arizona, USA
[b]Department of Biological Sciences, Northern Arizona University, Flagstaff, Arizona, USA
[c]Allarity Therapeutics, Hørsholm, Denmark

ABSTRACT By late 2020, the coronavirus disease 2019 (COVID-19) pandemic, caused by severe acute respiratory syndrome coronavirus 2 (SARS-CoV-2), had caused tens of millions of infections and over 1 million deaths worldwide. A protective vaccine and more effective therapeutics are urgently needed. We evaluated a new poly(ADP-ribose) polymerase (PARP) inhibitor, stenoparib, that recently advanced to phase II clinical trials for treatment of ovarian cancer, for activity against human respiratory coronaviruses, including SARS-CoV-2, *in vitro*. Stenoparib exhibits dose-dependent suppression of SARS-CoV-2 multiplication and spread in Vero E6 monkey kidney and Calu-3 human lung adenocarcinoma cells. Stenoparib was also strongly inhibitory to the human seasonal respiratory coronavirus HCoV-NL63. Compared to remdesivir, which inhibits viral replication downstream of cell entry, stenoparib impedes entry and postentry processes, as determined by time-of-addition (TOA) experiments. Moreover, a $10\,\mu M$ dosage of stenoparib—below the approximated $25.5\,\mu M$ half-maximally effective concentration (EC_{50})—combined with $0.5\,\mu M$ remdesivir suppressed coronavirus growth by more than 90%, indicating a potentially synergistic effect for this drug combination. Stenoparib as a stand-alone or as part of combinatorial therapy with remdesivir should be a valuable addition to the arsenal against COVID-19.

IMPORTANCE New therapeutics are urgently needed in the fight against COVID-19. Repurposing drugs that are either already approved for human use or are in advanced stages of the approval process can facilitate more rapid advances toward this goal. The PARP inhibitor stenoparib may be such a drug, as it is currently in phase II clinical trials for the treatment of ovarian cancer and its safety and dosage in humans have already been established. Our results indicate that stenoparib possesses strong antiviral activity against SARS-CoV-2 and other coronaviruses *in vitro*. This activity appears to be based on multiple modes of action, where both pre-entry and postentry viral replication processes are impeded. This may provide a therapeutic advantage over many current options that have a narrower target range. Moreover, our results suggest that stenoparib and remdesivir in combination may be especially potent against coronavirus infection.

KEYWORDS COVID-19, NL63, PARP, SARS-CoV-2, stenoparib

The novel severe acute respiratory syndrome coronavirus 2 (SARS-CoV-2) emerged from Wuhan, China, in late 2019, and rapidly spanned the globe in a devastating pandemic (1). Coronavirus disease 2019 (COVID-19) compromises the upper and lower respiratory systems and may affect all people (2). Although in many cases COVID-19

symptoms may be mild, some patients present with pulmonary distress, leading to severe lung damage, and treatment options are limited (1, 3–5). Mortality estimates range from 0.5% to more than 5% (6). According to the Johns Hopkins COVID Resource Center (7), as of 1 December 2020, over 15 million infections and more than 260,000 deaths due to COVID-19 have occurred in the United States alone, and the pandemic continues (8). A protective vaccine may soon be broadly available (1, 2), but unless sufficient immunity can be achieved in the population, COVID-19 has the potential to cause morbidity and mortality for years to come. To date, COVID-19 has largely been controlled through nonpharmaceutical measures such as quarantine, social isolation, and the use of personal protective equipment. Clearly, more efficacious treatments are needed.

Individuals who contract COVID-19 are most commonly infected by person-to-person transmission, where inhaled droplets containing infectious virions are seeded into the respiratory tract (1). The virions bind to respiratory epithelium via the affinity of the virus spike (S) complex to the angiotensin-converting enzyme 2 (ACE2) receptor (9). The cellular serine protease TMPRSS2 plays a pivotal role in S protein priming (10), which in turn facilitates fusion between the viral and cellular plasma membranes and internalization of the virus-receptor complex by endocytosis. Subsequently, the virus is uncoated and releases its single-stranded RNA genome, which is processed, translated, and replicated in the host cytosol. Copies of the viral genome are packaged into bilayer membrane envelopes, and these new infectious virions are exported from the cell (11, 12). The SARS-CoV-2 life cycle is typical of other coronaviruses, including the highly virulent SARS-CoV, the cause of severe acquired respiratory syndrome (SARS) (9). Conservation of key steps in the coronavirus viral life cycles potentially constitutes an "Achilles' heel" that is broadly susceptible to therapeutic intervention.

Antiviral therapeutics impede interactions between the virus and the host cell. Potential targets include virus binding to the cellular receptor, viral entry or virus-host membrane fusion, viral transcription, translation, replication, and export. (1). Stenoparib is an investigational, orally available small molecule that inhibits poly(ADP-ribose) polymerase (PARP), a key enzyme in DNA repair (13). Stenoparib is unique in that it has dual inhibitory activity against the PARP 1/2 and tankyrase 1/2 enzymes, which are important regulators of the canonical Wnt/β-catenin checkpoint, which is often dysregulated in metastatic breast cancer (14). Until August 2020, stenoparib was known as 2X-121 and previously as E7449. Recently, another PARP inhibitor, mefuparib (CVL218), was shown to inhibit SARS-CoV-2 *in vitro*. CVL218 suppressed SARS-CoV-2 infection in Vero E6 African green monkey cells (15). As implied by molecular modeling studies, CVL218 and other PARP inhibitors may block viral replication by interfering the viral nucleocapsid (N) protein binding to an RNA template (15).

The practice of repurposing existing drugs for new indications has advantages over developing an entirely new drug (16, 17). There are numerous repurposed drugs in use, including zidovudine, which was repurposed from the treatment of cancer to treat HIV/AIDS; the epilepsy drug topiramate, which is used to treat obesity; and aspirin for analgesia and the prevention of colorectal cancer, among other examples (16). With repurposing, the risk of failure is lower than developing a new drug, because safety trials have already been completed and the *in vivo* pharmacokinetics have been characterized; thus, cost and time of development are reduced. Moreover, the repurposing endeavor itself may reveal new disease targets and pathways. Altogether, repurposing can produce more rapid and efficient returns (16, 18). Stenoparib is currently in phase II clinical trials for the treatment of ovarian cancer (14). Based on the recent promising results of the PARP inhibitor CVL218 against SARS-CoV-2 *in vitro* (15), we evaluated the activity of stenoparib against SARS-CoV-2, with an eye toward its use as a treatment for COVID-19.

RESULTS

Stenoparib inhibits the replication of SARS-CoV-2 in Vero E6 cells. Based on the reported antiviral activity of other PARP inhibitors on SARS-CoV-2 *in vitro* (15), we
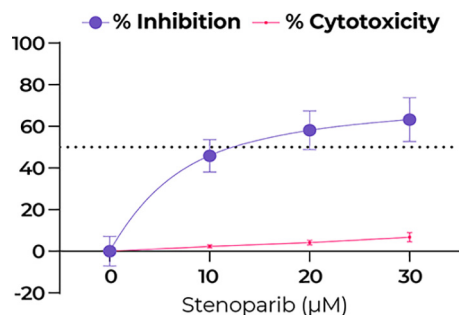
FIG 1 Stenoparib exhibits dose-dependent inhibition of SARS-CoV-2 as measured by RT-qPCR. RT-qPCR was performed on viral RNA collected from cell culture supernatants at 48 h postinfection. Replicates within each run were averaged, and a total of three experiments were performed. Error bars were based on averaged standard deviations within runs. Cytotoxicity against Vero E6 cells was determined at 48 h using the Promega CytoTox 96 assay kit, and values are the averages from two independent experiments (reported in Fig. 2A).

aimed to determine whether stenoparib possessed a similar activity against the virus. Stenoparib was prepared as a solution in dimethyl sulfoxide (DMSO) and used to treat Vero E6 cells infected with SARS-CoV-2 (USA-WA1/2020). Vero E6 is a common cell platform for propagating coronaviruses, including SARS-CoV-2 and SARS-CoV (19, 20). At 48 h after infection, RNA was isolated from cell supernatants, and viral copy number was estimated by reverse transcription quantitative real-time PCR (RT-qPCR). Viral RNA measurements were compared to those of untreated cell controls (estimated at 2.45×10^9 copies per ml; standard deviation [SD] $= 2.0 \times 10^5$) and of infected cells treated with a cocktail of camostat mesylate and E64d (C/E), which are protease inhibitors that impede processing of the virus spike protein and interfere with virus entry into the cell (10, 21). In parallel, we assessed potential toxic effects of stenoparib using the lactate dehydrogenase (LDH) release assay, which indicates cytotoxicity due to cell lysis. As shown in Fig. 1, stenoparib demonstrated dose-dependent activity against SARS-CoV-2 at concentrations up to 30 μM with negligible cytotoxicity. The significant 63.2% reduction in viral load following treatment ($t = 8.608$, $P = 0.0010$) is similar to the results reported for the CVL218 PARP inhibitor (35.2 to 99.7% inhibition) at comparable concentrations (15).

At concentrations higher than 30 μM and treatment durations exceeding 48 h, stenoparib displayed marked cytotoxicity to Vero E6 cells (Fig. 2A), which limited our capacity to comprehensively test the activity of the drug. We used a stenoparib response software predictor to preassess the susceptibility of human tumor cells based on the quantitative activity of 414 genes (22). When applied to human cell lines used with SARS-CoV-2 (23), the algorithm predicted that LLC-MK2 cells would be less sensitive to stenoparib toxicity than Vero E6 cells. The cell line Calu-3, originally isolated from the pleural effusion of a patient with lung adenocarcinoma (24), was predicted to be even more resistant than LLC-MK2. When these predictions were compared against a panel of 174 human cancer cell lines, Vero E6 was predicted to be highly sensitive (77th percentile), LLC-MK2 was predicted to be moderately sensitive (67th percentile), and Calu-3 was predicted to be less sensitive (49th percentile) (22). The decreased sensitivity of Calu-3 cells was verified using stenoparib concentrations up to 60 μM and exposure for up to 120 h, with no elevation in cytotoxicity over baseline conditions ($t = 8.237$, $P = 0.0144$) (Fig. 2B).

Calu-3 lung epithelial cells as a platform for SARS-CoV-2. Since Calu-3 cells were more resistant to the toxic effects of stenoparib than Vero E6 cells, we utilized Calu-3 to test the effectiveness of higher doses than were achievable with Vero E6. The viral plaque assay comprehensively assesses inhibitors on the viral intracellular life cycle, from virus entry to multiplication and cell-to-cell spread. Plaques result from cell damage and death following infection, appearing as empty regions, or "dead zones," in the
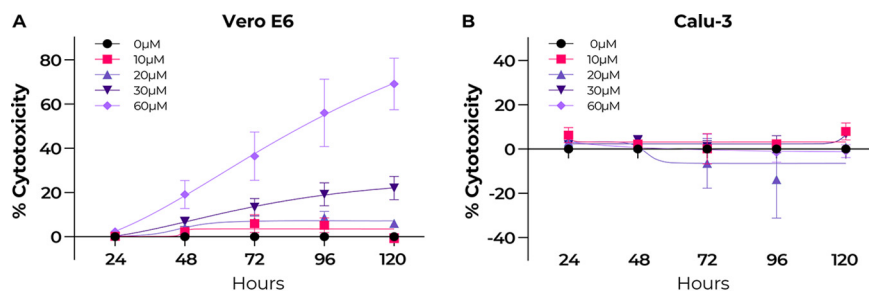
FIG 2 Stenoparib is cytotoxic in Vero E6 cells at concentrations greater than 30 μM but not in Calu-3 cells. Cytotoxicity was determined using the Promega CytoTox 96 lactate dehydrogenase release assay kit by harvesting culture medium every 24 h up to 120 h postexposure. (A) Vero E6 cells; (B) Calu-3 cells. Stenoparib concentrations used were 10, 20, 30, and 60 μM. Measurements were normalized to cells treated with 1.0% Triton X-100 and compared to untreated controls. Biological replicates from two runs were averaged, and median values are plotted. Results are representative of two experiments, and error bars are based on the standard deviation.

cell monolayer (25). Fresh medium containing 2% fetal bovine serum (FBS), with or without stenoparib or C/E control inhibitors, was applied to confluent monolayers of Calu-3 cells, which were then infected with SARS-CoV-2 for 1 h. At this time, the infection medium was removed, and the cells were overlaid with a semisolid matrix consisting of cell growth medium in 1.2% low-melting-temperature agarose, with or without stenoparib or control inhibitors. At 120 h postinfection, cells were fixed with paraformaldehyde and stained with crystal violet, and the number of plaques was visually counted. As shown in Fig. 3A (see also Fig. S1 in the supplemental material), treatment with 30 μM stenoparib resulted in a 30.6% reduction of PFU per well compared to infected, untreated cells ($t = 3.054$, $P = 0.0379$). Using a higher dose of 60 μM stenoparib, we observed nearly complete inhibition of plaque formation (94.0%; $t = 10.24$, $P = 0.0005$) with no significant cytotoxicity ($t = 0.446$, $P = 0.6992$), approaching the effect of the C/E control inhibitor (Fig. S1). These observations are mirrored by the results from RT-qPCR, which showed an 80.6% reduction of viral copy number with 60 μM stenoparib ($P < 0.0001$) compared to the untreated cell controls (estimated at 4.43×10^8 copies per ml; SD = 2.4×10^4). These observations affirm the prediction that Calu-3 cells are more resistant to the effects of stenoparib than Vero E6 cells and are suitable hosts for SARS-CoV-2 *in vitro*. It is interesting to speculate that Calu-3 cells may exhibit a degree of resistance to conditions that can be rapidly toxic in other, more rapidly dividing cell lines, which warrants further exploration. Indeed, the *in vitro* doubling time of Calu-3 cells (>60 h) was notably longer than that of either the Vero E6 (~24 h) or the LLC-MK2 (~36 h) cell line.

The NL63 virus as a surrogate *in vitro* model. In addition to SARS-CoV-2, several other human coronaviruses, including SARS-CoV, interact with human cells via the ACE2 receptor and multiply intracellularly utilizing similar pathways (9). This group includes the respiratory coronavirus HCoV-NL63 (also referred to as NL63), which is a cause of seasonal colds in humans. While symptoms are generally mild, NL63 infections can be serious in infants and immunocompromised individuals (26–28). Based on its relatedness to SARS-CoV-2, and to establish a surrogate system for use in biosafety level 2 (BSL-2) instead of BSL-3 laboratory conditions, we evaluated NL63 for testing the effects of stenoparib.

The NL63 virus (NR-470) was propagated in LLC-MK2 rhesus macaque kidney cells (29). Viral replication levels were assessed by plaque assay and RT-qPCR as performed for SARS-CoV-2. Controls were infected untreated cells and infected cells treated with the C/E inhibitor cocktail. Overall, the effects of stenoparib on NL63 corroborated the results of our experiments with SARS-CoV-2. Treatment resulted in a dose-dependent decrease in virus replication, achieving a 69.3% and 95.8% reduction of plaquing efficiency and viral copy number with 30 μM stenoparib, measured by plaque assay and
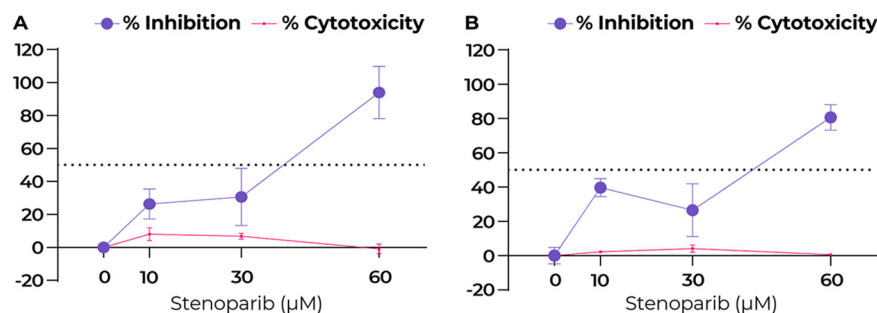
FIG 3 Stenoparib exhibits dose-dependent inhibition of SARS-CoV-2 in Calu-3 cells. (A) Plaque-forming efficiency using SARS-CoV-2. Values are normalized as a percentage of inhibition compared to infected but untreated cells. Plaques were counted 120 h after infection, replicates from each run were averaged, and assays were performed three times. Error bars are based on the standard deviation across all runs. (B) RT-qPCR was performed on viral RNA collected from cell culture supernatants at 48 h postinfection, and replicate values within each run were averaged; a total of three runs were performed. Error bars are based on averaged standard deviations within runs. Cytotoxicity against Calu-3 cells was determined at 48 and 120 h, as appropriate, using the Promega CytoTox 96 assay kit, and values represent the average of the two independent experiments (reported in Fig. 2B).

RT-qPCR, respectively, compared to untreated controls ($t = 7.982$ and 12.82; $P = 0.0002$ for both) (Fig. 4A and B).

Identifying effects of stenoparib on the coronavirus life cycle. Coronavirus inhibitors may target one or several intracellular growth stages, including virus entry (camostat mesylate and hydroxychloroquine), endosomal processing (hydroxychloroquine and rapamycin), translation and RNA processing (lopinavir), and transcription and replication (remdesivir) (1, 11, 30). By altering the time of addition (TOA) and duration of treatment *in vitro*, we can discern whether a drug affects virus entry, intracellular growth, or both. TOA experiments were conducted using the viral plaque assay with NL63 as a surrogate for SARS-CoV-2. RT-qPCR was performed in parallel to measure viral loads. We used remdesivir as a reference inhibitor, since its mechanism, target, and dosage range are known (31). Experiments to determine the life cycle stages affected by stenoparib were performed as follows: (i) to ascertain the effect on virus entry, cells were transiently exposed to compounds starting 1 h before infection and ending 1 h after infection; (ii) for effects on postentry events, including transcription, processing, translation, and replication, compounds were added 1 h after infection, when a number of virions would have already entered cells, and treatment was continued until the experimental endpoint at 120 h; (iii) to examine the maximum achievable effect of the compounds, a full-time assay was performed. Treatment was initiated simultaneously
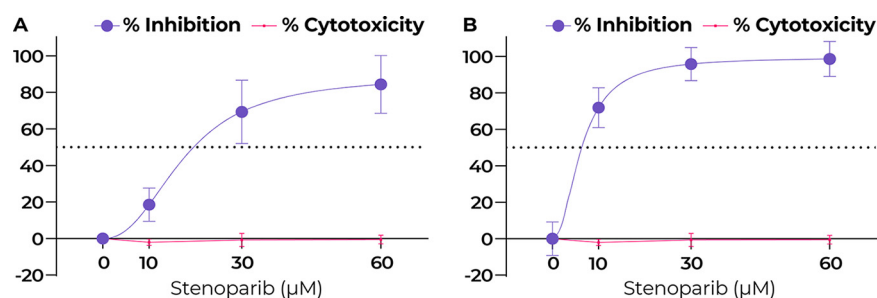
FIG 4 Stenoparib exhibits dose-dependent inhibition of HCoV-NL63 in LLC-MK2 cells. (A) Plaquing efficiency values are normalized as a percentage of inhibition compared to infected but untreated cells. Plaques were counted 120 h after infection, and assays were performed three times. Error bars are based on the standard deviation across all runs. (B) RT-qPCR was performed on viral RNA collected from cell culture media at 120 h postinfection. Biological replicates from each run were averaged, and three independent runs were performed. Error bars were based on averaged standard deviations within runs. Cytotoxicity against LLC-MK2 cells was determined at 120 h using the Promega CytoTox 96 assay kit, and values are averages from the three independent experiments.

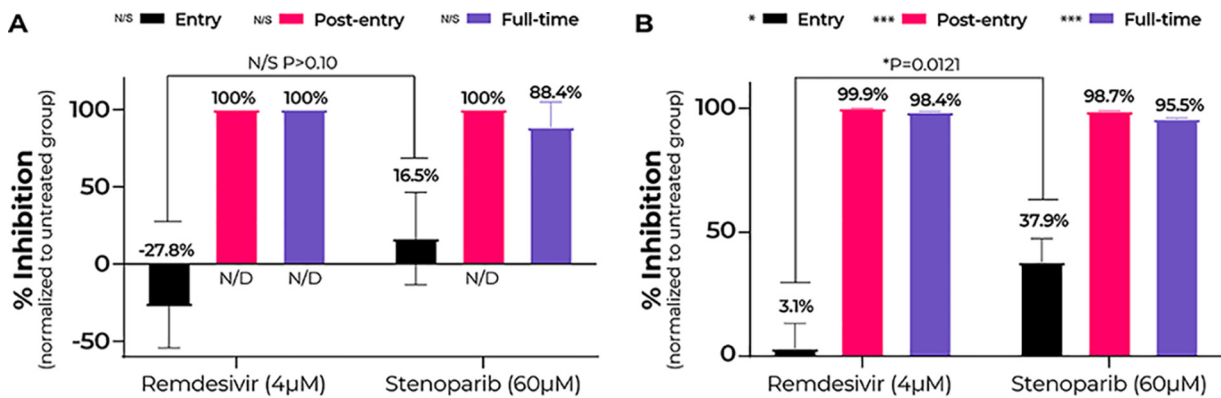**FIG 5** Stenoparib inhibits HCoV-NL63 entry and postentry events, while remdesivir inhibits postentry events. (A) Plaque assays were performed three times, and replicate PFU counts from each run were averaged. Error bars are based on standard deviation among runs. Brackets indicate the *t* test comparison and *P* value for the Entry group. No significant difference was observed between stenoparib and remdesivir under any treatment (N/S). "N/D" indicates that no plaques were detected. (B) RT-qPCR was performed on viral RNA collected from cell culture medium at 120 h postinfection, and replicate values within each run were averaged; a total of three runs were performed. Error bars were based on averaged standard deviations within runs. Brackets indicate the *t* test comparison and *P* value for the Entry group. Significant differences were observed between stenoparib and remdesivir for all treatments.

with virus infection and continued until the 120-h endpoint (see Materials and Methods for a detailed description).

As shown in Fig. 5A, the antiviral activity of stenoparib is most notable when added postinfection. The 60 μM stenoparib dose achieved complete inhibition of NL63 plaquing, with no detectable plaques following postentry treatment compared to untreated cells ($P < 0.0001$). This is on a par with the effect of 4 μM remdesivir, which also eliminated plaque formation. Likewise, assay results for the full-time treatment were comparable between stenoparib and remdesivir, with 88.4% reduction in plaque efficiency for stenoparib ($t = 5.582$, $P = 0.0051$) and full inhibition for remdesivir versus untreated cells. This is consistent with our results from RT-qPCR, where stenoparib produced 98.7% ($t = 9.988$, $P = 0.0099$) and 95.5% ($t = 9.663$, $P = 0.0105$) inhibition versus untreated controls for postentry and full-time drug exposure, and also comparable to the activity of remdesivir. These data are in line with those reported previously for the CVL218 PARP inhibitor and remdesivir (15).

With the plaque assay, we noticed a 16.5% reduction in plaque formation following transient treatment with stenoparib early in the infection time course (Fig. 5A, "Entry"). This effect was not markedly different from the results recorded for remdesivir (-27.8%; $t = 1.919$, $P = 0.1275$). Inhibition of virus entry is not expected for remdesivir, since its activity is specific to blocking of RNA replication (31, 32), which is a mid-late event in the viral life cycle. In contrast, our results from RT-qPCR strongly support a specific effect for stenoparib on inhibiting virus entry, where a 37.9% reduction in viral load is observed in the entry assay compared to just a 3.1% reduction for remdesivir ($t = 4.352$, $P = 0.0121$) (Fig. 5B). Effects on viral entry are consistent with the predicted activity of stenoparib on processes involved in early coronavirus infection events (see Discussion). Taken as a whole, these observations suggest that stenoparib may affect multiple targets that play roles in the early and late stages of coronavirus intracellular multiplication.

The combination of stenoparib and remdesivir strongly inhibits NL63. Combination drug therapies are widely used for the treatment for some of the worst human diseases, including cancer (33), HIV/AIDS (34), and multidrug-resistant tuberculosis (35). The strategy of combination therapy seeks to increase the beneficial effects of multiple drugs, lower their doses to reduce adverse effects, and minimize the induction of resistance (36). Generally, the activity of a drug combination is considered additive when the combined effect of two drugs is equivalent to their individual doses, while if the effect is less than additive, the combination is considered antagonistic. Synergy occurs
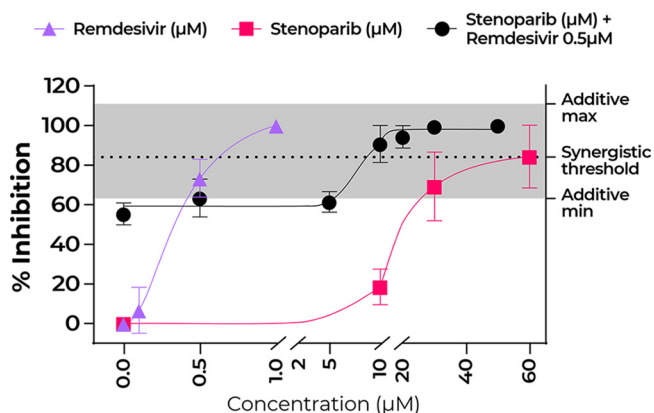
FIG 6 Stenoparib and remdesivir in combination is a potent inhibitor of NL63. Plaque assays were performed a minimum of two times, and replicate values from each run were averaged. Plaquing efficiency values are normalized as a percentage of inhibition compared to infected but untreated cells. Three data sets are plotted to illustrate the treatment of NL63 with stenoparib and remdesivir each as monotherapy and with both as combination therapy, whereby increasing concentrations of stenoparib are combined with $0.5\,\mu M$ remdesivir; the EC_{50} was computationally approximated at $0.46\,\mu M$. The stenoparib monotherapy data are the same as reported above (Fig. 4A). The synergistic activity threshold is defined as the sum of the mean values of $10\,\mu M$ stenoparib and $0.5\,\mu M$ remdesivir as monotherapies, while the gray highlighted area represents the minimum and maximum possible additive activity values based on the range of error for the same concentrations observed during these experiments.

when the combined effect is greater than the additive effect (36). Combinations of two or more drugs may lead to a synergistic effect by combining different mechanisms of action (MOA). Examples of synergistic combinations of drugs with distinct MOA include streptomycin-penicillin (37), trimethoprim-sulfa drugs (co-trimoxazole) (38), and β-lactam/β-lactamase inhibitor combinations such as amoxicillin-clavulanate (39) against bacterial infections.

Based on the fact that stenoparib and remdesivir inhibit coronavirus by distinct MOA (31, 32, 40), we approximated the half-maximal effective concentration (EC_{50}) of stenoparib and remdesivir as $25.5\,\mu M$ and $0.46\,\mu M$ using the NL63 virus and plaque assays. Calculations were aided by the online calculator from AAT Bioquest (Quest Graph EC50 Calculator; AAT Bioquest, Inc.; 26 October 2020; https://www.aatbio.com/tools/ec50-calculator). We hypothesized that a combination of stenoparib and remdesivir would be more potent than the individual compounds. To test this, we combined a range of doses of stenoparib with $0.5\,\mu M$ remdesivir and tested these for activity against NL63.

As shown in Fig. 6, complete inhibition of NL63 plaque formation was achieved with $60\,\mu M$ stenoparib, in line with our earlier results with SARS-CoV-2 and Calu-3 cells (Fig. 3). Complete inhibition was also achieved with $1.0\,\mu M$ remdesivir. However, a combination of $10\,\mu M$ stenoparib and $0.5\,\mu M$ remdesivir was more effective than either compound alone at these doses, achieving 90.7% inhibition for the combination, versus 18.5% inhibition for $10\,\mu M$ stenoparib and 65.6% for $0.5\,\mu M$ remdesivir, suggesting at least additive effects when the drugs are combined. Notably, the stenoparib dose ($10\,\mu M$) used in the combination is far below the compound's EC_{50} of $25.5\,\mu M$. Altogether, these results support investigating the use of stenoparib and remdesivir as a combinatorial therapy for SARS-family coronavirus infections.

DISCUSSION

Prior to the emergence of COVID-19, attempts to identify inhibitors of coronavirus were mainly focused on SARS-CoV and Middle East respiratory syndrome coronavirus (MERS-CoV). The recent efforts to develop COVID-19 therapeutics spans the gamut from new drug discovery to repurposing existing drugs. There are some excellent

reviews on the subject (17, 41). Here, we focus on the compound stenoparib, formerly known as 2X-121, an inhibitor of the cellular enzyme PARP-1/2. Stenoparib is thought to inhibit SARS-CoV-2 by multiple mechanisms, predominately by inhibiting of ADP-ribosylation of proteins required for virus replication and assembly (42). ADP-ribosylation is a conserved, posttranslational modification that is key for proper formation of the coronavirus nucleocapsid, and inhibition can negatively affect packaging of the viral genome and virion stability. Specific targets of ADP-ribosylation include viral nsp3 protein, which is essential for virulence and a component of the replication/transcription complex (RTC) (43, 44). Moreover, PARP inhibitors may exert additional protective effects at the host and cellular levels by reducing depletion of NAD^+ and ATP, which leads to cell necrosis (40), as well as decreasing the proinflammatory NF-κB-triggered cytokine storm, which can damage host organs (45). It has also been suggested that PARP inhibitors enhance the degradation of the host type I interferon receptor (IFN-1R), which would also have a modulatory effect on the host inflammatory response (46).

In this study, inhibition of SARS-family coronaviruses by stenoparib *in vitro* is likely due to interference with multiple stages of the virus life cycle. Consistent with its predicted activity against virus replication and assembly, stenoparib is effective when introduced postinfection. Additionally, we noted an association between stenoparib pretreatment and decreased virus counts soon after infection. This may reflect activity against additional targets, including those involved in virus entry. Stenoparib interference with tankyrase and Wnt/β-catenin signaling at the cell membrane may lead to dysregulation of a complex signaling pathway that could result in fewer numbers of virions entering the cell, for example by downregulation of the ACE2 receptor. The precise intracellular targets of stenoparib and its effect on virus entry and postentry processes is under investigation. In contrast, inhibition by remdesivir was predominately on postentry events; its effect on virus entry was minimal at best, which is consistent with its MOA of targeting virus replication machinery. Overall, our observations imply multiple mechanisms for stenoparib, including impeding of viral entry and intracellular growth via modifications of multiple viral and host proteins.

Other human coronaviruses that utilize ACE2 for binding and entry may be suitable as surrogate platforms for the study of SARS-CoV-2 *in vitro*, so long as they can be propagated in the laboratory and are able to elicit cellular infection phenotypes that can be quantitatively measured. We show that the human seasonal coronavirus NL63, which can cause a cold-like illness in humans (26), is such an example. Like SARS-CoV-2 and SARS-CoV, NL63 is internalized following the binding of viral S-complex proteins to the ACE2 receptor (28, 47–49). According to our observations, NL63 is susceptible to inhibition by compounds that affect SARS-CoV-2, including remdesivir, the protease inhibitors camostat mesylate and E64d, and stenoparib, the subject of this study. This result suggests that stenoparib possesses broad activity against seasonal as well as pandemic betacoronaviruses.

In light of the *in vitro* cytotoxic effects of stenoparib, we were unable to test it in Vero E6 cells against SARS-CoV-2 at doses exceeding 30 μM. Stenoparib was developed as a cytotoxic drug for cancer treatment (14), so it is not surprising that it showed dose-dependent cytotoxicity against rapidly dividing Vero E6 cells. PARP inhibitors typically express their lethality after several replication cycles (50). The susceptibility of Vero E6 cells to stenoparib toxicity may be linked to their fast-growing phenotype, since two replication cycles can be achieved in as little as 48 h. Although LLC-MK2 cells, which are utilized for propagation and testing of NL63, are substantially more resistant to stenoparib, their susceptibility to SARS-CoV-2 infection is suboptimal. We were thus presented with a conundrum as to how to test high doses of stenoparib against SARS-CoV-2 to assess its maximum activity. This was addressed through the use of the Calu-3 human lung carcinoma cell line to model SARS-CoV-2 infections. Our results confirm the suitability of Calu-3 as a host for SARS-CoV-2 and its high degree of resistance to stenoparib toxicity. This characteristic of Calu-3 cells was predicted *in silico* using a method previously employed on clinical tumor biopsy specimens (22), and experimentally

validated in this study. Infection of Calu-3 monolayers with SARS-CoV-2 formed large, clearly visible plaques, and in this regard, the performance of Calu-3 surpassed that of Vero E6. A notable characteristic of Calu-3 is its slow-growth properties, which may coincide with a general degree of resistance to compounds that target essential cellular pathways and are toxic to more rapidly dividing cells.

A promising drug to emerge from COVID therapeutic trials is the nucleoside analog remdesivir, which shows activity against phylogenetically diverse viruses, including Ebola virus, Nipah virus, respiratory syncytial virus (RSV), and coronaviruses such as SARS- and MERS-CoV (51), SARS-CoV-2 (31) and, as reported here, the seasonal human HCoV-NL63. Reviews on the MOA of remdesivir have been published (17, 41, 51). After entering the cell, remdesivir is triple phosphorylated to form remdesivir triphosphate, and this structure is thought to inhibit RNA polymerase, resulting in chain termination. While the precise molecular mechanism is not fully defined (51), the EC_{50} of remdesivir has been reported to be 0.77 μM for SARS-CoV-2 (31), which is in line with our measurement of 0.54 μM for SARS-CoV-2 and comparable to our experimentally determined EC_{50} of 0.46 μM against NL63.

While remdesivir inhibits the viral replicon, our data support multiple targets for stenoparib. Moreover, stenoparib and remdesivir may be a potent combination for inhibiting SARS-family coronaviruses inside cells. A mixture of 10 μM stenoparib and 0.5 μM remdesivir was more successful at inhibiting the NL63 virus than either compound alone at these doses. Notably, 10 μM stenoparib approaches the maximum tolerated dose of 5 μM observed during phase I clinical trials (22). Considering their distinct mechanisms and high potency, a combination of remdesivir and stenoparib is likely to produce a synergistic effect on additional SARS-family coronaviruses, including SARS-CoV-2. Studies involving this combination in susceptible COVID-19 animal models are in line for efficacy testing. Either alone or in combination with other antiviral drugs, PARP inhibitors provide the potential of a new therapeutic option for clinicians during the early viral replication stages of COVID-19 and, perhaps, in a prophylactic strategy in congregant living situations.

MATERIALS AND METHODS

The antiviral activity of stenoparib *in vitro* was assessed against the novel coronavirus SARS-CoV-2 isolate USA-WA1/2020 (NR-52281; BEI Resources, NIAID, NIH) and human coronavirus strain HCoV-NL63 (NR-470; BEI Resources, NIAID, NIH). We used Vero E6 cells (ATCC CRL-1586) and Calu-3 cells (ATCC HTB-55) from the American Type Culture Collection (ATCC, Manassas, VA, USA) in EMEM (Eagle's minimum essential medium) supplemented with 2% or 10% fetal bovine serum (FBS), 100 U/ml penicillin, 100 μg/ml streptomycin (Pen-Strep), 0.01 M HEPES, 1 mM sodium pyruvate, 1$\times$ nonessential amino acids solution (SH3023801; Thermo Fisher), and 2 mM L-glutamine, for the propagation and experimentation with SARS-CoV-2. LLC-MK2 cells (ATCC CCL-7), maintained in medium 199 (M4530, Millipore Sigma) supplemented with FBS and Pen-Strep, were used for the experiments with the NL63 coronavirus. Inhibition of viral replication was assessed using reverse-transcription quantitative real-time PCR (RT-qPCR) to measure the number of virions released into the cellular supernatant.

Plaque assays. Six-well plates (CLS3516; Millipore Sigma) were seeded with $\sim$3.0 $\times$ 10^5 cells/well and incubated for 48 to 72 h at 37°C in 5% CO_2 until 80 to 90% confluence was reached. Calu-3 cells were incubated for >10 days to achieve 80 to 90% confluence. Prior to infection, the medium was replaced with fresh medium containing 2% FBS with various concentrations of stenoparib as appropriate for each experiment (see Results) and infected with coronavirus (SARS-CoV-2 or NL63) at a multiplicity of infection (MOI) of 0.013 for SARs-CoV-2 and 0.003 for NL63. Medium was then replaced with a 1$\times$ Dulbecco's MEM (DMEM, Millipore Sigma)/1.2% low-melting-point agarose (Bio-Rad) overlay containing the appropriate drug concentration for each experiment. This was allowed to solidify at room temperature for 15 min and incubated for 120 h at 37°C in a 5% CO_2 atmosphere. A cocktail of the protease inhibitors camostat mesylate and E64d (C/E) was a control for all experiments (21). SARS-CoV-2 manipulations were conducted in a BSL-3 facility. First, 2.0 ml of 4% paraformaldehyde was added to each overlay for 30 min, followed by staining with 1% crystal violet, removal of the overlay, and a triple rinse with phosphate-buffered saline (PBS). PFU were counted, averaged, and normalized to the untreated control group. Each run contained three biological replicates and was conducted a minimum of two times. Standard deviation was calculated using the variation of averaged counts among all runs. Values were plotted using GraphPad Prism version 8.0.0 for Windows (GraphPad Software) and annotated using Adobe Illustrator (Adobe Systems Incorporated). Statistical significance was determined using a parametric unpaired *t* test in GraphPad Prism version 8.0.0.

RT-qPCR. (i) Infection and viral RNA extraction. Twelve-well plates (CLS3513; Millipore Sigma) were seeded with $\sim$1.0 $\times$ 10^5 cells/well and incubated until 80 to 90% confluence was reached. Growth

medium was replaced and infected with coronavirus (SARS-CoV-2 or NL63) at an MOI of 0.04 for SARs-CoV-2 and 0.01 for NL63 for up to 120 h at 37°C in 5% CO_2 atmosphere. C/E was used as a control inhibitor for all experiments. Each run contained two biological replicates and was conducted three times. A 400-μl portion of supernatant was harvested at 48 h for SARS-CoV-2 and at 120 h for NL63. RNA was extracted using Invitrogen Pure-Link RNA kits (Thermo Fisher) according to their recommendations.

(ii) Signature identification and qPCR assay design. Two TaqMan qPCR assays were designed for SARS-CoV-2 and NL63. For NL63, the reference genome (NC_005831) was divided into 200-nucleotide fragments, which were aligned against a set of 2,771 coronavirus genomes with BLAT v36.2 (52) in conjunction with LS-BSR v1.2.2 (53). Regions were identified that had a BLAST score ratio (BSR) (54) of $\geq$0.8 in 60 NL63 genomes and a BSR of <0.4 in all other coronavirus genomes. A total of 10 fragments were highly specific to all NL63 genomes. Primers and probes were identified using Primer3 v2.3.6 (55). A similar process was conducted for SARS-CoV-2 assay design, except that the GCF_009858895.2 reference genome was used. A total of 4 fragments were unique to 64 distinct SARS-CoV-2 genomes. A probe was designed targeting the spike (S) protein furin cleavage site with Primer3.

The SARS-CoV-2 qPCR amplified a 125-bp region of the S protein using forward primer CoV2-S_19F (5′-GCTGAACATGTCAACAACTC-3′) and reverse primer CoV2-S_143R (5′-GCAATGATGGATTGACTAGC-3′) with MGB TaqMan probe CoV2-S_93FP (5′-ACTAATTCTCCTCGGCGGGC-3′) labeled with the dye 6-carboxyfluorescein (FAM), which was designed based on the SARS-CoV-2 genome GCF_009858895.2 (GenBank accession no. MN908947.3), while the NL63 qPCR amplified a 191-bp region of a membrane protein (GenBank accession no. YP_003770.1) using forward primer NL63_10F (5′-TGGTCGCTCTGTT AATGAAA-3′) and reverse primer NL63_200R (5′-AAATTTCTTCCTAGCAGCTC-3′) with MGB TaqMan probe NL63_102RP (5′-CCCTCCTGAGAGGCAACACC-3′), labeled with the dye VIC, which was based on the HCoV-NL63 genome (GenBank accession no. MN306040.1).

(iii) Reverse transcription and PCR amplification. We initially used a two-step method where viral RNA was converted into cDNA using Invitrogen SuperScript IV VILO master mix (11766500; Thermo Fisher) in a 96-well format (18021-014; Thermo Fisher) in a SimpliAmp thermocycler (Applied Biosystems). One microliter of template cDNA was then subjected to qPCR in 10-μl reaction mixtures containing 1× TaqMan Universal master mix II (without AmpERASE UNG), with a 0.2 μM concentration of each forward and reverse primer and a 0.1 μM concentration of probe for the SARS-CoV-2 qPCR and a 0.25 μM concentration of each forward and reverse primer and a 0.125 μM concentration of probe for the NL63 qPCR. Amplification was performed in triplicate using either a QuantStudio 7 Flex or QuantStudio 12K system (Applied Biosystems), as follows: 10 min at 95°C, then 40 cycles of 95°C for 15 s and 60°C for 1 min. Another approach employed a one-step procedure in which viral RNA was converted to cDNA using the TaqMan primers, followed by qPCR (4× Reliance one-step multiplex RT-qPCR Supermix) with the same primers, probes, and concentrations as for the two-step approach. Triplicate reactions were performed using QuantStudio under the following conditions: 50°C for 10 min, 95°C for 10 min, and 40 cycles of 95°C for 10 s and 60°C for 30 s. Positive amplification and nontemplate controls were included on every run.

(iv) Data analysis. Synthetic double-stranded DNA fragments were generated (gBlocks gene fragments; Integrated DNA Technologies) as qPCR controls; they contained amplification primers for either SARS-CoV-2 or NL63 targets and were elongated to 200 bp. These gBlocks were resuspended according to the manufacturer's protocol, quantified using a Qubit 4 fluorometer with a dsDNA HS assay kit (Q32851; Thermo Fisher), and then normalized to 10^8 copies per μl. Using serial dilution, we were able to extrapolate viral copy number in each of the experimental samples. Based on these standards, the QuantStudio instrument software generated a curve to quantify sample reactions. The calculated quantities for each sample were averaged, and the standard deviation was calculated among reactions. Values for the experimental replicates and the standard deviations among experimental runs were averaged and then normalized to the untreated control group to obtain percent inhibition values. These were plotted using GraphPad Prism version 8.0.0 for Windows, and annotations were added using Adobe Illustrator. Where appropriate, statistical significance was determined using a parametric unpaired t test in GraphPad Prism version 8.0.0.

Cytotoxicity. Cytotoxicity was measured using the Promega CytoTox 96 nonradioactive cytotoxicity assay kit (G1780) in 50-μl reaction mixtures according to the manufacturer's protocol. The absorbance at 490 nm (A_{490}) was measured using a BioTek Synergy HT plate reader, model no. 7091000. Relative cytotoxicity was calculated by dividing the experimental LDH release as measured at 490 nm by the maximum LDH release control multiplied by 100.

Time-of-addition experiments. For the full-time experiments, virus, drug and cells were incubated for 1 h. Medium was then replaced with fresh medium containing the drug. For entry experiments, cells were pretreated with drug for 1 h and then infected with virus for an additional hour, followed by medium replacement that lacked drug. Postentry experiments utilized cells that were infected with virus for 1 h, and medium was replaced with fresh medium containing the drug. Statistical significance was determined using a parametric unpaired t test in GraphPad Prism version 8.0.0.

Stenoparib in combination with remdesivir. We performed plaque assays and used the data to estimate the EC_{50} of stenoparib and remdesivir (329511; MedKoo Biosciences, Morrisville, NC, USA) against NL63 (both drugs) and SARS-CoV-2 (remdesivir only) in LLC-MK2 and Vero E6 cells according to results from at least two experimental runs. The EC_{50} values were approximated with the aid of the online calculator from AAT Bioquest (Quest Graph EC50 Calculator; 26 October 2020; https://www.aatbio .com/tools/ec50-calculator).

SUPPLEMENTAL MATERIAL

ACKNOWLEDGMENTS

REFERENCES

1. Hu B, Guo H, Zhou P, Shi ZL. 2020. Characteristics of SARS-CoV-2 and COVID-19. Nature Rev Microbiol https://doi.org/10.1038/s41579-020-00459-7.
2. Wu ZY, McGoogan JM. 2020. Characteristics of and important lessons from the coronavirus disease 2019 (COVID-19) outbreak in China. Summary of a rReport of 72 314 cases from the Chinese Center for Disease Control and Prevention. JAMA 323:1239–1242. https://doi.org/10.1001/jama.2020.2648.
3. Liu Y, Mao B, Liang S, Yang JW, Lu HW, Chai YH, Wang L, Zhang L, Li QH, Zhao L, He Y, Gu XL, Ji XB, Li L, Jie ZJ, Li Q, Li XY, Lu HZ, Zhang WH, Song YL, Qu JM, Xu JF, Treatment SC. 2020. Association between age and clinical characteristics and outcomes of COVID-19. Eur Respir J 55:2001112. https://doi.org/10.1183/13993003.01112-2020.
4. Wu C, Chen X, Cai Y, Xia J, Zhou X, Xu S, Huang H, Zhang L, Zhou X, Du C, Zhang Y, Song J, Wang S, Chao Y, Yang Z, Xu J, Zhou X, Chen D, Xiong W, Xu L, Zhou F, Jiang J, Bai C, Zheng J, Song Y. 2020. Risk factors associated with acute respiratory distress syndrome and death in patients with coronavirus disease 2019 pneumonia in Wuhan, China (vol 180, pg 934, 2020). JAMA Intern Med 180:934–1031. https://doi.org/10.1001/jamainternmed.2020.0994.
5. Guan W, Ni Z, Hu Y, Liang W, Ou C, He J, Liu L, Shan H, Lei C, Hui DSC, Du B, Li L, Zeng G, Yuen KY, Chen R, Tang C, Wang T, Chen P, Xiang J, Li S, Wang JL, Liang Z, Peng Y, Wei L, Liu Y, Hu YH, Peng P, Wang JM, Liu J, Chen Z, Li G, Zheng Z, Qiu S, Luo J, Ye C, Zhu S, Zhong N, Grp CMTE, China Medical Treatment Expert Group for Covid-19. 2020. Clinical characteristics of coronavirus disease 2019 in China. N Engl J Med 382:1708–1720. https://doi.org/10.1056/NEJMoa2002032.
6. Dong E, Du H, Gardner L. 2020. An interactive web-based dashboard to track COVID-19 in real time. Lancet Infect Dis 20:533–534. https://doi.org/10.1016/S1473-3099(20)30120-1.
7. Johns Hopkins University of Medicine Coronavirus Resource Center. 2020. COVID tracker. https://www.arcgis.com/apps/opsdashboard/index.html#/409af567637846e3b5d4182fcd779bea.
8. Team IC-F. 2020. Modeling COVID-19 scenarios for the United States. Nat Med https://doi.org/10.1038/s41591-020-1132-9.
9. Rabi FA, Al Zoubi MS, Kasasbeh GA, Salameh DM, Al-Nasser AD. 2020. SARS-CoV-2 and coronavirus disease 2019: what we know so far. Pathogens 9:231. https://doi.org/10.3390/pathogens9030231.
10. Hoffmann M, Kleine-Weber H, Schroeder S, Kruger N, Herrler T, Erichsen S, Schiergens TS, Herrler G, Wu NH, Nitsche A, Muller MA, Drosten C, Pohlmann S. 2020. SARS-CoV-2 cell entry depends on ACE2 and TMPRSS2 and is blocked by a clinically proven protease inhibitor. Cell 181:271–280. E8. https://doi.org/10.1016/j.cell.2020.02.052.
11. Poduri R, Joshi G, Jagadeesh G. 2020. Drugs targeting various stages of the SARS-CoV-2 life cycle: exploring promising drugs for the treatment of Covid-19. Cell Signal 74:109721. https://doi.org/10.1016/j.cellsig.2020.109721.
12. Astuti I, Ysrafil. 2020. Severe acute respiratory syndrome coronavirus 2 (SARS-CoV-2): an overview of viral structure and host response. Diabetes Metab Syndr 14:407–412. https://doi.org/10.1016/j.dsx.2020.04.020.
13. Dziadkowiec KN, Gąsiorowska E, Nowak-Markwitz E, Jankowska A. 2016. PARP inhibitors: review of mechanisms of action and BRCA1/2 mutation targeting. Prz Menopauzalny 15:215–219. https://doi.org/10.5114/pm.2016.65667.
14. McGonigle S, Chen ZH, Wu JY, Chang P, Kolber-Simonds D, Ackermann K, Twine NC, Shie JL, Miu JZT, Huang KC, Moniz GA, Nomoto K. 2015. E7449: a dual inhibitor of PARP1/2 and tankyrase1/2 inhibits growth of DNA repair deficient tumors and antagonizes Wnt signaling. Oncotarget 6:41307–41323. https://doi.org/10.18632/oncotarget.5846.

15. Ge Y, Tian T, Huang S, Wan F, Li J, Li S, Yang H, Hong L, Wu N, Yuan E, Cheng L, Lei Y, Shu H, Feng X, Jiang Z, Chi Y, Guo X, Cui L, Xiao L, Li Z, Yang C, Miao Z, Tang H, Chen L, Zeng H, Zhao D, Zhu F, Shen X, Zeng J. 2020. A data-driven drug repositioning framework discovered a potential therapeutic agent targeting COVID-19. bioRxiv https://doi.org/10.1101/2020.03.11.986836:2020.03.11.986836.
16. Pushpakom S, Iorio F, Eyers PA, Escott KJ, Hopper S, Wells A, Doig A, Guilliams T, Latimer J, McNamee C, Norris A, Sanseau P, Cavalla D, Pirmohamed M. 2019. Drug repurposing: progress, challenges and recommendations. Nat Rev Drug Discov 18:41–58. https://doi.org/10.1038/nrd.2018.168.
17. Saha RP, Sharma AR, Singh MK, Samanta S, Bhakta S, Mandal S, Bhattacharya M, Lee SS, Chakraborty C. 2020. Repurposing drugs, ongoing vaccine, and new therapeutic development initiatives against COVID-19. Front Pharmacol 11:1258. https://doi.org/10.3389/fphar.2020.01258.
18. Zhou YD, Hou Y, Shen JY, Huang Y, Martin W, Cheng FX. 2020. Network-based drug repurposing for novel coronavirus 2019-nCoV/SARS-CoV-2. Cell Discov 6:14. https://doi.org/10.1038/s41421-020-0153-3.
19. Qinfen Z, Jinming C, Xiaojun H, Huanying Z, Jicheng H, Ling F, Kunpeng L, Jingqiang Z. 2004. The life cycle of SARS coronavirus in Vero E6 cells. J Med Virol 73:332–337. https://doi.org/10.1002/jmv.20095.
20. Ogando NS, Dalebout TJ, Zevenhoven-Dobbe JC, Limpens R, van der Meer Y, Caly L, Druce J, de Vries JJC, Kikkert M, Barcena M, Sidorov I, Snijder EJ. 2020. SARS-coronavirus-2 replication in Vero E6 cells: replication kinetics, rapid adaptation and cytopathology. J Gen Virol 101:925–940. https://doi.org/10.1099/jgv.0.001453.
21. Li J, Zhan P, Liu X. 2020. Targeting the entry step of SARS-CoV-2: a promising therapeutic approach. Signal Transduct Target Ther 5:98. https://doi.org/10.1038/s41392-020-0195-x.
22. Plummer R, Dua D, Cresti N, Drew Y, Stephens P, Foegh M, Knudsen S, Sachdev P, Mistry BM, Dixit V, McGonigle S, Hall N, Matijevic M, McGrath S, Sarker D. 2020. First-in-human study of the PARP/tankyrase inhibitor E7449 in patients with advanced solid tumours and evaluation of a novel drug-response predictor. Br J Cancer 123:525–533. https://doi.org/10.1038/s41416-020-0916-5.
23. Chu H, Chan JF, Yuen TT, Shuai H, Yuan S, Wang Y, Hu B, Yip CC, Tsang JO, Huang X, Chai Y, Yang D, Hou Y, Chik KK, Zhang X, Fung AY, Tsoi HW, Cai JP, Chan WM, Ip JD, Chu AW, Zhou J, Lung DC, Kok KH, To KK, Tsang OT, Chan KH, Yuen KY. 2020. Comparative tropism, replication kinetics, and cell damage profiling of SARS-CoV-2 and SARS-CoV with implications for clinical manifestations, transmissibility, and laboratory studies of COVID-19: an observational study. Lancet Microbe 1:e14–e23. https://doi.org/10.1016/S2666-5247(20)30004-5.
24. Fogh J, Fogh JM, Orfeo T. 1977. One hundred and twenty-seven cultured human tumor cell lines producing tumors in nude mice. J Natl Cancer Inst 59:221–226. https://doi.org/10.1093/jnci/59.1.221.
25. Baer A, Kehn-Hall K. 2014. Viral concentration determination through plaque assays: using traditional and novel overlay systems. J Vis Exp 2014:e52065. https://doi.org/10.3791/52065.
26. van der Hoek L, Pyrc K, Berkhout B. 2006. Human coronavirus NL63, a new respiratory virus. FEMS Microbiol Rev 30:760–773. https://doi.org/10.1111/j.1574-6976.2006.00032.x.
27. Glowacka I, Bertram S, Herzog P, Pfefferle S, Steffen I, Muench MO, Simmons G, Hofmann H, Kuri T, Weber F, Eichler J, Drosten C, Pohlmann S. 2010. Differential downregulation of ACE2 by the spike proteins of severe acute respiratory syndrome coronavirus and human coronavirus NL63. J Virol 84:1198–1205. https://doi.org/10.1128/JVI.01248-09.

28. Li W, Sui J, Huang IC, Kuhn JH, Radoshitzky SR, Marasco WA, Choe H, Farzan M. 2007. The S proteins of human coronavirus NL63 and severe acute respiratory syndrome coronavirus bind overlapping regions of ACE2. Virology 367:367–374. https://doi.org/10.1016/j.virol.2007.04.035.

29. Schildgen O, Jebbink MF, de Vries M, Pyrc K, Dijkman R, Simon A, Muller A, Kupfer B, van der Hoek L. 2006. Identification of cell lines permissive for human coronavirus NL63. J Virol Methods 138:207–210. https://doi.org/10.1016/j.jviromet.2006.07.023.

30. Omarjee L, Janin A, Perrot F, Laviolle B, Meilhac O, Mahe G. 2020. Targeting T-cell senescence and cytokine storm with rapamycin to prevent severe progression in COVID-19. Clin Immunol 216:108464. https://doi.org/10.1016/j.clim.2020.108464.

31. Wang M, Cao R, Zhang L, Yang X, Liu J, Xu M, Shi Z, Hu Z, Zhong W, Xiao G. 2020. Remdesivir and chloroquine effectively inhibit the recently emerged novel coronavirus (2019-nCoV) in vitro. Cell Res 30:269–271. https://doi.org/10.1038/s41422-020-0282-0.

32. Chang CK, Jeyachandran S, Hu NJ, Liu CL, Lin SY, Wang YS, Chang YM, Hou MH. 2016. Structure-based virtual screening and experimental validation of the discovery of inhibitors targeted towards the human coronavirus nucleocapsid protein. Mol Biosyst 12:59–66. https://doi.org/10.1039/c5mb00582e.

33. Bigioni M, Benzo A, Irrissuto C, Lopez G, Curatella B, Maggi CA, Manzini S, Crea A, Caroli S, Cubadda F, Binaschi M. 2008. Antitumour effect of combination treatment with sabarubicin (MEN 10755) and cis-platin (DDP) in human lung tumour xenograft. Cancer Chemother Pharmacol 62:621–629. https://doi.org/10.1007/s00280-007-0645-y.

34. Casado JL, Banon S. 2015. Dutrebis (lamivudine and raltegravir) for use in combination with other antiretroviral products for the treatment of HIV-1 infection. Expert Rev Clin Pharmacol 8:709–718. https://doi.org/10.1586/17512433.2015.1090873.

35. Caminero JA, Sotgiu G, Zumla A, Migliori GB. 2010. Best drug treatment for multidrug-resistant and extensively drug-resistant tuberculosis. Lancet Infect Dis 10:621–629. https://doi.org/10.1016/S1473-3099(10)70139-0.

36. Garcia-Fuente A, Vazquez F, Vieitez JM, Garcia Alonso FJ, Martin JI, Ferrer J. 2018. CISNE: an accurate description of dose-effect and synergism in combination therapies. Sci Rep 8:4964. https://doi.org/10.1038/s41598-018-23321-6.

37. Reynolds B, Rowley D. 1953. Synergism between streptomycin and penicillin. Br J Exp Pathol 34:651–655.

38. Nichols RJ, Sen S, Choo YJ, Beltrao P, Zietek M, Chaba R, Lee S, Kazmierczak KM, Lee KJ, Wong A, Shales M, Lovett S, Winkler ME, Krogan NJ, Typas A, Gross CA. 2011. Phenotypic landscape of a bacterial cell. Cell 144:143–156. https://doi.org/10.1016/j.cell.2010.11.052.

39. Yogev R, Melick C, Kabat WJ. 1981. In vitro and in vivo synergism between amoxicillin and clavulanic acid against ampicillin-resistant Haemophilus influenzae type b. Antimicrob Agents Chemother 19:993–996. https://doi.org/10.1128/aac.19.6.993.

40. Kouhpayeh S, Shariati L, Boshtam M, Rahimmanesh I, Mirian M, Zeinalian M, Salari-Jazi A, Khanahmad N, Damavandi MS, Sadeghi P, Khanahmad H. 2020. The molecular story of COVID-19; NAD+ depletion addresses all questions in this infection. Preprints https://doi.org/10.20944/preprints202003.0346.v1.

41. Pillaiyar T, Meenakshisundaram S, Manickam M. 2020. Recent discovery and development of inhibitors targeting coronaviruses. Drug Discov Today 25:668–688. https://doi.org/10.1016/j.drudis.2020.01.015.

42. Grunewald ME, Fehr AR, Athmer J, Perlman S. 2018. The coronavirus nucleocapsid protein is ADP-ribosylated. Virology 517:62–68. https://doi.org/10.1016/j.virol.2017.11.020.

43. Lei J, Kusov Y, Hilgenfeld R. 2018. Nsp3 of coronaviruses: structures and functions of a large multi-domain protein. Antiviral Res 149:58–74. https://doi.org/10.1016/j.antiviral.2017.11.001.

44. Fehr AR, Athmer J, Channappanavar R, Phillips JM, Meyerholz DK, Perlman S. 2015. The nsp3 macrodomain promotes virulence in mice with coronavirus-induced encephalitis. J Virol 89:1523–1536. https://doi.org/10.1128/JVI.02596-14.

45. Gharote MA. 2020. Role of poly (ADP) ribose polymerase-1 inhibition by nicotinamide as a possible additive treatment to modulate host immune response and prevention of cytokine storm in COVID-19. Int J Mol Sci 72:25–28. https://doi.org/10.25259/Int.J.Mol.Sci_29_2020.

46. Coperchini F, Chiovato L, Croce L, Magri F, Rotondi M. 2020. The cytokine storm in COVID-19: an overview of the involvement of the chemokine/chemokine-receptor system. Cytokine Growth Factor Rev 53:25–32. https://doi.org/10.1016/j.cytogfr.2020.05.003.

47. Smith MK, Tusell S, Travanty EA, Berkhout B, van der Hoek L, Holmes KV. 2006. Human angiotensin-converting enzyme 2 (ACE2) is a receptor for human respiratory coronavirus NL63. Adv Exp Med Biol 581:285–288. https://doi.org/10.1007/978-0-387-33012-9_48.

48. Pohlmann S, Gramberg T, Wegele A, Pyrc K, van der Hoek L, Berkhout B, Hofmann H. 2006. Interaction between the spike protein of human coronavirus NL63 and its cellular receptor ACE2. Adv Exp Med Biol 581:281–284. https://doi.org/10.1007/978-0-387-33012-9_47.

49. Lin HX, Feng Y, Wong G, Wang L, Li B, Zhao X, Li Y, Smaill F, Zhang C. 2008. Identification of residues in the receptor-binding domain (RBD) of the spike protein of human coronavirus NL63 that are critical for the RBD-ACE2 receptor interaction. J Gen Virol 89:1015–1024. https://doi.org/10.1099/vir.0.83331-0.

50. Garnett MJ, Edelman EJ, Heidorn SJ, Greenman CD, Dastur A, Lau KW, Greninger P, Thompson IR, Luo X, Soares J, Liu Q, Iorio F, Surdez D, Chen L, Milano RJ, Bignell GR, Tam AT, Davies H, Stevenson JA, Barthorpe S, Lutz SR, Kogera F, Lawrence K, McLaren-Douglas A, Mitropoulos X, Mironenko T, Thi H, Richardson L, Zhou W, Jewitt F, Zhang T, O'Brien P, Boisvert JL, Price S, Hur W, Yang W, Deng X, Butler A, Choi HG, Chang JW, Baselga J, Stamenkovic I, Engelman JA, Sharma SV, Delattre O, Saez-Rodriguez J, Gray NS, Settleman J, Futreal PA, Haber DA, et al. 2012. Systematic identification of genomic markers of drug sensitivity in cancer cells. Nature 483:570–575. https://doi.org/10.1038/nature11005.

51. Saha A, Sharma AR, Bhattacharya M, Sharma G, Lee SS, Chakraborty C. 2020. Probable molecular mechanism of remdesivir for the treatment of COVID-19: need to know more. Arch Med Res 51:585–586. https://doi.org/10.1016/j.arcmed.2020.05.001.

52. Kent WJ. 2002. BLAT—the BLAST-like alignment tool. Genome Res 12:656–664. https://doi.org/10.1101/gr.229202.

53. Sahl JW, Caporaso JG, Rasko DA, Keim P. 2014. The large-scale blast score ratio (LS-BSR) pipeline: a method to rapidly compare genetic content between bacterial genomes. PeerJ 2:e332. https://doi.org/10.7717/peerj.332.

54. Raska DA, Myers GS, Ravel J. 2005. Visualization of comparative genomic analyses by BLAST score ratio. BMC Bioinformatics 6:2. https://doi.org/10.1186/1471-2105-6-2.

55. Rozen S, Skaletsky H. 2000. Primer3 on the WWW for general users and for biologist programmers. Methods Mol Biol 132:365–386. https://doi.org/10.1385/1-59259-192-2:365.